Provided for non-commercial research and education use.
Not for reproduction, distribution or commercial use.

This article appeared in a journal published by Elsevier. The attached copy is furnished to the author for internal non-commercial research and education use, including for instruction at the authors institution and sharing with colleagues.

Other uses, including reproduction and distribution, or selling or licensing copies, or posting to personal, institutional or third party websites are prohibited.

In most cases authors are permitted to post their version of the article (e.g. in Word or Tex form) to their personal website or institutional repository. Authors requiring further information regarding Elsevier's archiving and manuscript policies are encouraged to visit:

http://www.elsevier.com/copyright

Author's personal copy

Earth and Planetary Science Letters 288 (2009) 268–278

Contents lists available at ScienceDirect

Earth and Planetary Science Letters

journal homepage: www.elsevier.com/locate/epsl

High efficiency of natural lamellar remanent magnetisation in single grains of ilmeno-hematite calculated using Mössbauer spectroscopy

Catherine A. McCammon [a,*], Suzanne A. McEnroe [b], Peter Robinson [b], Karl Fabian [b], Benjamin P. Burton [c]

[a] Bayerisches Geoinstitut, Universität Bayreuth, D-95440 Bayreuth, Germany
[b] Geological Survey of Norway, N-7491 Trondheim, Norway
[c] National Institute of Standards and Technology, Gaithersburg, MD 20899, USA

ARTICLE INFO

Article history:
Received 25 June 2009
Received in revised form 11 August 2009
Accepted 17 September 2009
Available online 12 October 2009

Editor: P. DeMenocal

Keywords:
hematite
ilmenite
lamellar magnetism
nanoparticles
NRM
magnetic anomalies

ABSTRACT

Rocks from large remanent magnetic anomalies on Earth have been found to contain exsolved rhombohedral oxides, which also have been proposed as earth analogues for the rocks creating the observed large remanent anomalies on Mars. Theoretical considerations and previous case studies of natural rocks have shown that the natural magnetisation is carried by lamellar magnetism due to uncompensated moments at the interface between antiferromagnetic hematite and paramagnetic ilmenite. Here, single grains (≈250 μm) of titanohematite with ferri-ilmenite exsolution lamellae from Mesoproterozoic metamorphic rock samples in southwest Sweden and the Adirondack Mountains, USA, are studied using room-temperature Mössbauer spectroscopy to identify possible characteristic magnetic signatures of lamellar magnetism. Mössbauer spectra of synthetic samples of titanohematite ($Fe_{0.95}Ti_{0.05}O_3$ and $Fe_{0.9}Ti_{0.1}O_3$) were collected for comparison and showed a dominant six-line magnetic spectrum due to Fe^{3+} in titanohematite with a weak sextet due to Fe^{2+}–Fe^{3+} charge transfer. Mössbauer spectra of the natural ilmeno-hematite grains are similar to those for synthetic titanohematite, but contain additionally two paramagnetic doublets corresponding to Fe^{2+} and Fe^{3+} in ilmenite. However, several grains also contain an additional weak, broad magnetic component that we assign to iron in contact layers according to the lamellar magnetism model. Similar to the previous Mössbauer results for natural hemo-ilmenite, there is no evidence for superparamagnetic behaviour of the nanoscale titanohematite lamellae contained within coarser ferri-ilmenite lamellae, and no evidence for single-domain or superparamagnetic magnetite. The compositions of titanohematite and ferri-ilmenite in the individual ilmeno-hematite grains calculated from the Mössbauer area ratios show that compositions are closer to end-member values than the compositions inferred from electron microprobe and transmission electron microscopy on the same grains, consistent with observations that lamella thicknesses are as small as a few nm. Bulk compositions of ilmeno-hematite grains calculated from the Mössbauer data confirm that the Swedish samples are significantly more ilmenite-rich than the Adirondack samples, and agree with an estimation of bulk composition through point counting of electron backscatter images. The Mössbauer data allow a quantitative estimation of contact layer abundance, which is used to determine the efficiency of lamellar natural remanent magnetisation acquisition. Because minerals with a high natural remanent magnetisation efficiency are expected to create larger remanent magnetic anomalies, contact layer abundance determination by Mössbauer spectroscopy provides a valuable new tool for mineral-based magnetic anomaly interpretation on Earth and other planetary bodies.

© 2009 Elsevier B.V. All rights reserved.

1. Introduction

1.1. Ilmeno-hematite as a natural remanence carrier

Ilmeno-hematite is the mineralogical name applied to a titanohematite host ($FeTiO_3$-bearing Fe_2O_3 solid solution) containing exsolution lamellae of ferri-ilmenite (Fe_2O_3-bearing $FeTiO_3$ solid solution). Ilmeno-hematite is abundant in oxidised metamorphic rocks on Earth, but also is a potential remanence carrier on other planets. The unusually intense and stable natural remanent magnetisation (NRM) of rocks containing ilmeno-hematite was highlighted many decades ago as a source of distinctive magnetic anomalies over Mesoproterozoic metamorphic rocks of the Adirondack Mountains, New York (Balsley and Buddington, 1954, 1957, 1958). More recently the Adirondack rocks (McEnroe and Brown, 2000) and similar Mesoproterozoic metamorphic rocks from southwest Sweden (McEnroe et al., 2001) have been studied in detail for their magnetic properties in relation to the associated remanent magnetic anomalies. These studies included reflected-light microscopy, electron microprobe analysis (EMPA) of

* Corresponding author. Tel.: +49 921 553709; fax: +49 921 553769.
E-mail address: catherine.mccammon@uni-bayreuth.de (C.A. McCammon).

0012-821X/$ – see front matter © 2009 Elsevier B.V. All rights reserved.
doi:10.1016/j.epsl.2009.09.030

Author's personal copy

constituent minerals, transmission electron microscopy (TEM) to investigate exsolution microstructures at the nanometre level, TEM-EDS (energy dispersive spectroscopy) analyses to estimate phase compositions at the submicron level (McEnroe and Brown, 2000; McEnroe et al., 2001, 2002; Kasama et al., 2004), and high- and low-temperature magnetic properties (943 K and 10 K). All results indicate a strong relation between exsolution microstructures and unusually strong and stable remanent magnetisation.

1.2. Lamellar magnetism

Inquiry into the physical origin of these strong remanences led to the concept of lamellar magnetism (LM; Robinson et al., 2002), which has been theoretically investigated by atomic Monte Carlo and density functional simulations of the magnetic properties of lamellar interfaces (Harrison and Becker, 2001; Robinson et al., 2002, 2004; Pentcheva and Nabi, 2008). The experimental proof that the natural magnetic remanence originates from nanoscale lamellae formed during slow cooling (Fabian et al., 2008) is based on the discovery of giant exchange bias below 50 K in some ilmeno-hematite bearing rocks (McEnroe et al., 2007a; Harrison et al., 2007; Fabian et al., 2008). Exchange bias requires the magnetic moment to be linked to exchange-coupled interfaces which here occur between the host and the lamellae.

1.3. Mössbauer spectroscopy on ilmeno-hematite

The magnetic properties of ilmeno-hematite minerals are entirely due to the site occupancies, valences of Fe ions, and magnetic interactions in the oxide-mineral structures and intergrowths. Therefore, Mössbauer spectroscopy is a natural approach to study the relation between nanoscale lamellae and host material. Previous Mössbauer investigations of hemo-ilmenite (ilmenite with hematite exsolution) at room temperature (Dyar et al., 2004), room- and low-temperature (Frandsen et al., 2007) and their magnetic properties (McEnroe et al., 2002, 2007b) have highlighted features interpreted to be due to magnetic interactions at the contact layers. The present work is the first Mössbauer study of ilmeno-hematite of metamorphic origin, and further, it uses a novel milliprobe technique (McCammon et al., 1991) to examine single grains extracted from polished rock thin sections. This approach was required because the selected rocks have only a small percentage of magnetic oxides, and, although the magnetic remanence of these rocks is dominated by ilmeno-hematite, some samples also contain multi-domain magnetite that would add further components to the Mössbauer spectra and reduce the possibility of a unique deconvolution.

1.4. Efficiency of lamellar natural remanent magnetisation

The Mössbauer results presented here provide a method to quantify the amount of contact layers at lamellar interfaces inside the ilmeno-hematite minerals. In combination with bulk magnetic measurements, this allows us to calculate the efficiency of NRM acquisition for a lamellar magnetic material. In agreement with a previous estimate from low-temperature exchange bias (Fabian et al., 2008), this efficiency turns out to be an order of magnitude larger than the typical efficiency of thermoremanent-magnetisation acquisition in single-domain (SD) magnetite. This explains the occurrence of large remanent magnetic anomalies over rocks containing lamellar magnetism oxides. It also may provide valuable information for the interpretation of Mössbauer measurements from planetary material in terms of its potential link to remanent magnetic anomalies. In addition, fundamental knowledge of the physical environment of Fe in ilmeno-hematite contact layers may have technological importance for the design of thin films based on ilmenite–hematite intergrowths, particularly where large exchange bias derives from the exchange coupling across the interface.

2. Experimental methods

2.1. Description of natural samples

Four natural ilmeno-hematite samples (S17, S19, S47 and AD34) were selected for this study, where extensive aeromagnetic surveys, as well as laboratory measurements on individual rock samples (magnetic properties, TEM, electron microprobe) had already been made. The fractions of rhombohedral oxides and magnetite were estimated using point-counted modes, supplemented by measurements of magnetic susceptibility which can be linked to magnetite content. NRM and susceptibility were measured on inch-core samples (cylinders of 2.54 cm width and height), and thin sections were subsequently cut from these cores.

Samples S17 and S19 are from a mafic body in the pyroxene-granulite region near Gödestad in southwestern Sweden. The texture and contact relations of the body suggest it was originally a gabbro or diorite that was either originally an oxidised igneous rock, or was oxidised by externally derived fluids, and then subjected to granulite-facies regional metamorphism. Pyroxene exsolution characteristics suggest the samples were subjected to prolonged annealing around 600 °C (McEnroe et al., 2001). At about this temperature, the oxides appear to have been homogeneous intermediate titanohematite, ferri-ilmenite, and end-member magnetite. The presently observed exsolution in hematite and ilmenite occurred on cooling below 520 °C, and electron microprobe and TEM analyses of sample S19 have been reported in McEnroe et al. (2001). The present study concentrates on selected grains of ilmeno-hematite (Fig. 1a,b). Modal analyses of samples S17 and S19 show ≈3% rhombohedral oxide and 1% multi-domain magnetite. Their NRM values of ≈18 A/m are extremely high for metamorphic rocks, whereas susceptibility values of ≈0.04 (SI) are common for granulite-grade rocks. Samples S17 and S19 lose little remanence by alternating field demagnetisation up to 100 mT, and both have high unblocking temperatures between 550 °C and 630 °C. Hysteresis measurements of mineral separates of ilmeno-hematite show bulk coercivities $H_C > 150$ mT.

S47-4 was one of several samples of hornblende-plagioclase amphibolite from the amphibolite-facies zone in southwestern Sweden, which lies northwest of the granulite-facies zone and separated from it by a “Mylonite Zone”. It may have a similar origin to the mafic rocks of the granulite-facies zone, but with a more hydrous subsequent metamorphism. In sample S47-4 there are only two host oxides, titanohematite, now extensively exsolved (Fig. 1d), and end-member magnetite. Within the ilmeno-hematite there are minor grains (some black dots in Fig. 1d) of corundum within ilmenite exsolution lamellae. Locally, there are minute needles of rutile which appear to have formed prior to ilmenite exsolution. Titanite rims surround ilmeno-hematite grains, probably formed at lower temperatures than the dominant oxide exsolution. Point counting of sample S47-4 yielded 0.61% oxide, of which 0.11% is magnetite and 0.5% is ilmeno-hematite. S47 has the same magnetic characteristics as S17 and S19: hardness, high unblocking temperature and stable magnetisation. The NRM and susceptibility values are 3.3 A/m and 0.012 (SI), respectively.

Sample AD34-1 is a microcline–sillimanite gneiss from the Russell Belt of the Adirondack Highlands near the boundary between the amphibolite-facies region of the Lowlands and the granulite-facies region of the Highlands. Its chemistry and mineralogy suggest that it originated as a rhyolitic lava or tuff that suffered hydrothermal alteration and/or weathering, resulting in significant removal of alkalis (hence the sillimanite) and oxidation before metamorphism. The dominant oxide in the microcline–sillimanite gneiss is again ilmeno-hematite, a titanohematite host with fine ilmenite exsolution (Fig. 1c), with minor rutile and rare magnetite. Eight samples from the same location (AD34) were measured for magnetic properties, and electron microprobe analyses of samples AD34-6 and AD34-7 are

Author's personal copy

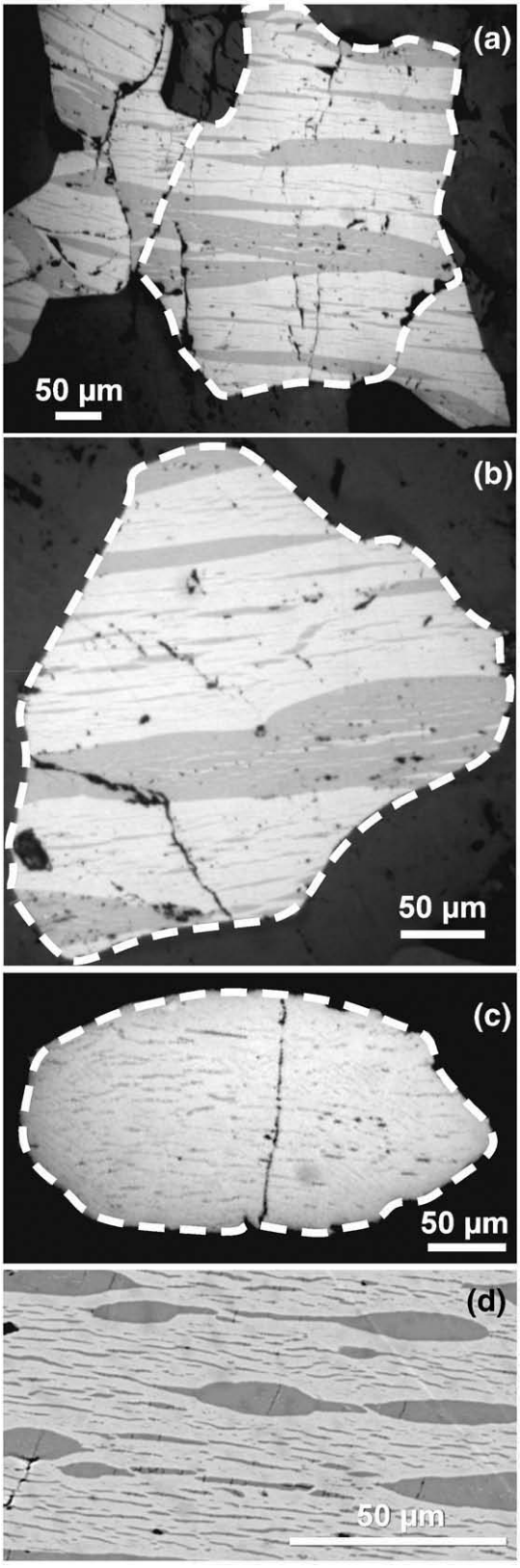

Fig. 1. (a)–(c) Optical photomicrographs in reflected light of single ilmeno-hematite grains of titanohematite host (light grey) containing ilmenite lamellae (dark grey) from samples (a) S19.5 (grain #2), (b) S17.2 (grain #2) and (c) AD-34-1 (grain #2). The small black areas are due to, Al-spinel, corundum, cracks or holes. The Mössbauer spectra taken from the regions enclosed by the white dashed lines are shown in Fig. 3a–c. (d) Backscattered electron image for titanohematite (light grey) S47-4 containing ilmenite lamellae (dark grey). The grain analysed by Mössbauer spectroscopy was from the same rock sample, but from a different thin section.

reported by McEnroe and Brown (2000). TEM analyses of sample AD34-5 and AD34-4 were performed by Kasama et al. (2004). The oxide compositions and observed exsolution lamellae are similar in all samples. NRM and susceptibility values for AD34-1 are 8.1 A/m and 0.00042 (SI), respectively. Unblocking temperatures are above 600 °C for all AD34 samples. No magnetite was observed in thin section AD34-1, which is in good agreement with the very low susceptibility values and high unblocking temperatures. Similar to the Swedish samples, alternating field demagnetisation to 100 mT has little effect on the NRM, and bulk coercivities exceed 150 mT.

2.2. Description of synthetic samples

Synthetic samples of titanohematite with nominal compositions $Fe_{0.95}Ti_{0.05}O_3$ (Ilm_{10}) and $Fe_{0.9}Ti_{0.1}O_3$ (Ilm_{20}) were made as part of the thesis work of Burton (1982). Samples were synthesized from dried Fe_2O_3, TiO_2 (anatase, partly transformed to rutile) and Fe-sponge (Johnson Matthey and Co. Limited) and a correction was made for oxidation of the Fe-sponge. Intimate mixtures of these constituents were prepared by: 1) grinding in an agate mortar under ethanol to avoid oxidation; 2) drying under a heat lamp; 3) wrapping in silver foil and sealing in silica tubes that were simultaneously heated and evacuated. The silica tubes were then annealed at 900–920 °C for at least 1 week, quenched in air, reground and re-annealed at 900–920 °C for at least one more week. The resulting fine-grained powders were X-rayed and appeared at that time to be single-phase hematite–ilmenite solid solution with no detectable pseudobrookite or magnetite solid solution phase(s). Using higher precision X-ray diffraction equipment (T. Boffa Ballaran, pers. comm. 2006), both these samples were found to contain about 1% magnetite.

2.3. Mössbauer spectroscopy

Exsolved ilmeno-hematite grains in the natural samples were identified on thin sections using optical microscopy, and the individual grains were removed intact using the commercially available Medenbach microdrill mounted on a polarising microscope. A selection of grains from each sample is shown in Fig. 1. Each grain was mounted on a mylar sheet using clear nail varnish, and masked with 25 μm thick Ta foil (absorbs 99% of 14.4 keV γ-rays) containing a hole with diameter in the range of 200–500 μm depending on the size of the grain, resulting in areas of 0.03–0.2 mm^2 that were measured using Mössbauer spectroscopy. From the grain thickness (≈30 μm) and an estimated composition, the dimensionless Mössbauer thickness of each sample was estimated to be roughly 3, which corresponds to approximately 7 mg Fe/cm^2. One of the ilmeno-hematite grains (S17-2 grain #1) was subsequently discovered to be associated with a small amount of magnetite, so a Mössbauer spectrum was recorded over a smaller area of the grain to concentrate the magnetite (S17-2 grain #1 m).

Synthetic titanohematite samples were ground, mixed with benzophenone to avoid preferred orientation, and loaded into Plexiglas sample holders with 12 mm diameter. Sample weights were chosen such that the dimensionless Mössbauer thickness was 2, which corresponds to approximately 5 mg Fe/cm^2.

Mössbauer spectra were recorded at room temperature (293 K) in transmission mode on a constant acceleration Mössbauer spectrometer fitted with either a nominal 1.85 GBq ^{57}Co conventional source in a 6 μm thick Rh matrix (synthetic samples) or a nominal 370 MBq ^{57}Co high specific activity point source in a 12 μm thick Rh matrix (single grains). The velocity scale was calibrated relative to 25 μm thick α-Fe foil using the positions certified for (former) National Bureau of Standards standard reference material no. 1541; line widths of 0.28 mm/s (conventional source) and 0.36 mm/s (point source) for the outer lines of α-Fe were obtained at room temperature. Spectra took 1 to 2 days each to collect, and were fitted using the

Author's personal copy

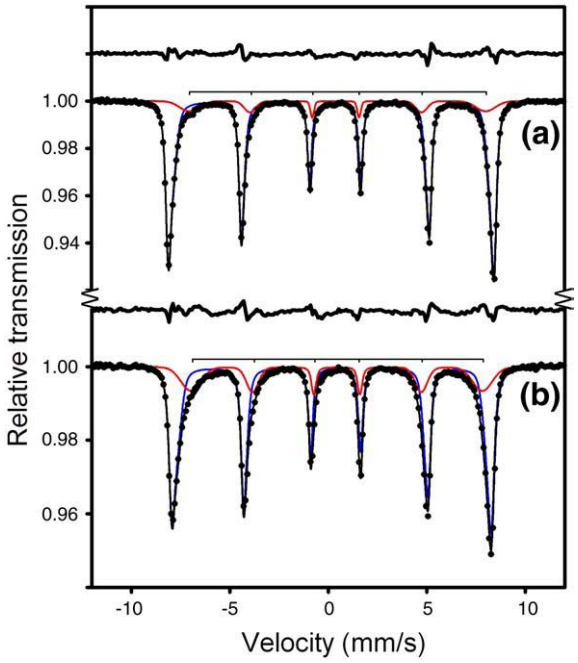

Fig. 2. Room-temperature Mössbauer spectra of synthetic polycrystalline titanohematite: (a) $Fe_{0.95}Ti_{0.05}O_3$; (b) $Fe_{0.9}Ti_{0.1}O_3$. The spectra were fit using a Voigt-based fitting analysis incorporating magnetic sextets for Fe^{3+} in titanohematite (blue online) and a single Voigt magnetic sextet for $Fe^{2.5+}$ in titanohematite (red online; line positions indicated above spectrum). The relative areas of the $Fe^{2.5+}$ sub-spectra yield ilmenite compositions that agree with the nominal chemical compositions (Table 1) when the Fe^{2+} abundance is taken to be 50% of the $Fe^{2.5+}$ absorption and Ti is calculated according to the substitution reaction 2 $Fe^{3+} \leftrightarrow Fe^{2+} + Ti^{4+}$. The residual (difference between experimental and calculated data) is shown above each spectrum, and is plotted on the same vertical scale as the spectra. (For interpretation of the references to color in this figure legend, the reader is referred to the web version of this article.)

commercially available fitting programme NORMOS written by R.A. Brand (distributed by Wissenschaftliche Elektronik GmbH, Germany).

3. Results

3.1. Synthetic samples

Mössbauer spectra of synthetic Ilm10 and Ilm20 are similar to those previously reported (Warner et al., 1972), and show a magnetic sextet corresponding to Fe^{3+} in $(Fe,Ti)_2O_3$ with pronounced broadening on the inside shoulders of the outer peaks, resulting in an asymmetric lineshape (Fig. 2). We fit the Fe^{3+} in $(Fe,Ti)_2O_3$ contribution using a Voigt-based fitting analysis (Rancourt and Ping, 1991) incorporating magnetic sextets, and the additional contribution to a magnetic sextet with Voigt lineshape. The small amount of magnetite that was detected by X-ray diffraction does not have an observable influence on the Mössbauer spectra, where the overlap of lines 5 and 6 of the magnetite spectrum (which contain peaks from both the B and A sites) with lines 5 and 6 of the hematite peaks would cause enhanced intensity near +5 and +8 mm/s. The hyperfine parameters that could be meaningfully determined from the spectra are given in Table 1.

Low-temperature magnetic measurements from 300 to 10 K show that these samples have no Morin transition, exactly as expected for a Ti-substituted hematite (Ericsson et al., 1986). Therefore the spins lie in the basal plane perpendicular to [0001], and are in the spin-canted configuration.

The mean magnetic hyperfine field of the Fe^{3+} subspectrum is lower than the value for pure Fe_2O_3 (52.1 T; van der Woude and Dekker, 1966), consistent with a reduction of the hyperfine field at the Fe^{3+} site due to substitution of non-magnetic Ti^{4+} in the crystal structure. The additional component has a centre shift intermediate between the value for Fe^{3+} and Fe^{2+}, and is assigned to Fe^{2+}–Fe^{3+} electron transfer taking place on a time-scale faster than the Mössbauer effect ($\approx 10^{-8}$ s) as suggested by Warner et al. (1972) based on their Mössbauer data and by Ishikawa (1958) based on high observed electrical conductivities. The relative amount of Fe^{2+} is calculated as half of the area of the additional component based on the valence state $Fe^{2.5+}$, where the relative area is divided equally between Fe^{2+} and Fe^{3+}. This procedure yields compositions based on the substitution mechanism 2 $Fe^{3+} \leftrightarrow Fe^{2+} + Ti^{4+}$ that are consistent with the nominal chemical compositions (Tables 1 and 2). Thus for Ilm10, $Fe^{3+}{}_{0.9}Fe^{2+}{}_{0.05}Ti_{0.05}O_3$ is 0.90/0.95 = 0.947 Fe^{3+} and 0.05/0.95 = 0.053 Fe^{2+}. Combining 0.053 Fe^{2+} with 0.053 Fe^{3+} gives 0.106 $Fe^{2.5+}$, leaving 0.894 Fe^{3+} which agrees with the Fe^{3+} relative area from Mössbauer data in Table 1. For Ilm20 the corresponding figures are 0.889 Fe^{3+} and 0.111 $Fe^{2+}$and 0.222 $Fe^{2.5+}$ and 0.777 Fe^{3+}, also in agreement with Table 1. All sextets were fit assuming ideal component ratios (3:2:1:1:2:3) which are valid for absorbers with random crystallites in the thin absorber approximation. This assumption appears to be consistent with the observed data (Fig. 2).

Table 1
Hyperfine parameters derived from room temperature Mössbauer data.

Sample	Grain #	Fe^{3+} in hematite					$Fe^{2.5+}$ in hematite				Fe^{2+} in ilmenite				Fe^{3+} in ilmenite
		δ	<2ε>	<B>	A_{23}	A	δ	2ε	B	A	δ	ΔE_Q	Γ	A	A
		mm/s	mm/s	T		%	mm/s	mm/s	T	%	mm/s	mm/s	mm/s	%	%
Ilm10	–	0.38	−0.21	50.7	*2*	89(2)	0.55	0.09	47	11(2)					
Ilm20	–	0.39	−0.22	49.7	*2*	77(3)	0.54	−0.01	46	23(3)					
S17-2	1	0.37	−0.20	49.6	1.9	52(5)	*0.54*	*0.07*	*46*	11(4)	1.03	0.70	0.41	31(3)	6(3)
	1 m	0.42	−0.28	50.0	1.6	83(10)					1.10	0.89	0.30	17(10)	
	2	0.38	−0.24	49.8	1.9	64(4)	*0.54*	*0.07*	*46*	6(3)	1.02	0.74	0.37	27(3)	4(2)
	3	0.39	−0.23	50.2	2.1	69(4)	*0.54*	*0.07*	*46*	3(3)	1.04	0.78	0.35	25(3)	3(3)
S19-5	1	0.34	−0.22	49.6	3.2	71(6)					0.99	0.62	1.25	29(6)	
	2	0.38	−0.22	49.7	2.0	58(3)	*0.54*	*0.07*	*46*	5(3)	1.02	0.71	0.38	30(3)	7(3)
	3	0.38	−0.22	49.9	2.2	64(3)	*0.54*	*0.07*	*46*	6(3)	1.04	0.73	0.31	28(3)	3(3)
AD34-1	1	0.38	−0.22	50.3	2.0	82(3)	*0.54*	*0.07*	*46*	7(2)	1.06	0.84	0.52	10(2)	1(1)
	2	0.37	−0.23	50.6	3.5	86(4)	*0.54*	*0.07*	*46*	9(3)	0.94	0.88	0.52	6(2)	0(1)
S47-3	–	0.38	−0.21	50.4	2.0	74(4)	*0.54*	*0.07*	*46*	6(3)	1.05	0.72	0.39	19(2)	2(1)
e.s.d.		0.02	0.02	0.5	0.2		0.05	0.10	2		0.05	0.05	0.05		

Notes:
[a]δ: centre shift relative to α-Fe; 2ε: quadrupole shift; *B*: hyperfine magnetic field; A_{23}: area ratio of line 2 to line 3; *A*: relative area; ΔE_Q: quadrupole splitting; Γ: full width at half maximum; e.s.d.: estimated standard deviation;<*N*>: weighted mean value of parameter *N*.
[b]Values in italics were fixed during the fitting process.

Author's personal copy

Table 2
Chemical compositions from Mössbauer data compared with other methods.

Sample	Grain #	Titanohematite(%"ilm")			Ferri-ilmenite(%"ilm")			Bulk (%"ilm")	
		Möss	EMPA	TEM	Möss	EMPA	TEM	Möss	PC
Ilm10	–	10(1)							
Ilm20	–	21(2)							
S17-2	avg		24[1]			93[1]			
	1	16(6)			92(6)			54(6)	
	2	8(4)			93(4)			47(6)	
	3	4(4)			95(6)			43(6)	
S19-5	avg		21 − 25[2]	16 ± 3[2]		88 − 90[2]	88 ± 4[2]		
	2	8(4)			90(5)			50(5)	
	3	8(4)			95(6)			48(6)	
AD34-1	avg		3-28[3]	8-12[4]		70-97[3]	93-100[4]		
	1	8(2)			95(7)			24(5)	
	2	9(3)			100(14)			19(7)	
S47-3	avg		16-20[1]			91-95[1]			40
	–	7(4)			95(3)			36(5)	

Notes:
Möss: Mössbauer spectroscopy; EMPA: electron microprobe analysis; TEM: transmission electron microscopy; PC: point counting.
[a]"ilm": $R^{2+}Ti^{4+}O_3$; Möss: Mössbauer spectroscopy; PC: point counting.
[b]"avg" indicates measurements made on grains from the same rock, but different to the grains examined using Mössbauer spectroscopy.
[c]References for EMPA and TEM data: [1] this work; [2] McEnroe et al. (2001); [3] McEnroe and Brown (2000); [4] Kasama et al. (2004).

3.2. Natural samples

The Mössbauer spectra of natural ilmeno-hematite grains (Fig. 3) show many similarities with the spectra from synthetic samples; hence a similar fitting approach was used. We fit the titanohematite contribution to the fitting model described above, with the lineshape and peak positions of the $Fe^{2.5+}$ sextet fixed to the values from synthetic $Fe_{0.95}Ti_{0.05}O_3$. Because the ilmeno-hematite grains could have preferred orientation, we allowed the component area ratios (A_{23}) of the middle (lines 2 and 5) to the inner peaks (lines 3 and 4) of the Fe^{3+} sextet to deviate from the ideal ratio of 2.0 for thin absorbers with randomly oriented crystallites. The Mössbauer spectra also show a quadrupole doublet arising from Fe^{2+} in ilmenite, with a shoulder on the low-velocity side likely due to Fe^{3+} in the same phase (Frandsen et al., 2007). The components of the ilmenite doublet could also be unequal due to preferred orientation, but unfortunately due to the low intensity of the ilmenite doublet and the strong overlap of components in the central region of the spectrum, it was not possible to obtain a robust solution when the ilmenite component area ratio was allowed to freely vary. However we conducted several fitting trials with different fixed values of the ilmenite component area ratio, and found that results (particularly the relative area of the ilmenite doublet) were unchanged within the given uncertainties. For the final fits, we accordingly added two Lorentzian quadrupole doublets with conventional constraints (equal component areas and widths), and due to the low intensity of the Fe^{3+} in ilmenite doublet we added the following constraints: (1) equal widths of the Fe^{2+} and Fe^{3+} ilmenite doublets; (2) peak positions of the Fe^{3+} ilmenite doublet constrained to literature values (Frandsen et al., 2007). Two of the spectra came from unusual grains (S17-2 grain #1 m was specifically chosen for the presence of a small quantity of magnetite, and S19-5 grain #1 showed extremely broad lines, perhaps due to lattice strain), and were fit to only a single magnetic sextet (Fe^{3+} in titanohematite) and a single doublet (Fe^{2+} in ilmenite). The hyperfine parameters derived from all fits are listed in Table 1.

Fe^{3+} in natural titanohematite has hyperfine parameters similar to those of the synthetic samples, with reduced values of the hyperfine magnetic field due to Ti^{4+} substitution and negative quadrupole shifts typical for the spin-canted structure. Most of the grains yield the ideal A_{23} value within experimental error, with the exception of two which show values greater than 3 (Table 1) (neglecting the grain containing magnetite). This likely arises due to preferred orientation of the magnetic quantisation axis to lie on average close to parallel to the plane of the thin section (i.e., perpendicular to the direction of the γ-rays). The spectrum of the grain containing a small quantity of magnetite (S17-2 grain #1 m) resembled those of other ilmeno-hematite grains, but with enhanced intensity of lines 5 and 6. These lines are the ones most affected by the overlap of a multi-domain magnetite spectrum with a titanohematite spectrum, where lines 5 and 6 of magnetite (containing contributions from both the A and the B sites) coincide with lines 5 and 6 of titanohematite. Both multi-domain magnetite and ilmeno-hematite grains are in the area analysed in this Mössbauer spectrum.

There is a deviation of the residual (difference between experimental and calculated data) from a horizontal line, most notably for sample S47-4 (Fig. 3d), but the deviation is also present in most other spectra from natural ilmeno-hematite grains. The most likely explanation is the presence of an additional broad magnetic component. We carried out several trial fits in order to: (1) assess the statistical significance of including the magnetic component in the fit using an F test (e.g., Bevington, 1969); (2) estimate the amount of the magnetic component that could be present in each spectrum; (3) assess the influence of including the magnetic component on the derived hyperfine parameters of the titanohematite and ilmenite components. One such trial fit of two of the spectra is illustrated in Fig. 4. From these trials we established the following: (1) inclusion of the magnetic component in the fit is statistically significant in spectra from Fig. 3a,b and d to at least the 99% level, but not the spectrum from Fig. 3c; (2) the magnetic component could not be fitted at all to the spectra of synthetic titanohematite (Fig. 2a–b); (3) the relative areas of the magnetic component in the natural ilmeno-hematite spectra vary from 4 to 16%; (4) the detection limit of the magnetic component based on the scatter of the baseline is estimated to be 5% of the total area; (5) although the hyperfine parameters (centre shift, hyperfine field, line-width) of the magnetic component cannot be determined uniquely, the relative areas between different fitting models do not vary outside the stated uncertainties and the hyperfine parameters of the other components in the spectra (titanohematite and ilmenite) are unchanged within their uncertainties.

4. Discussion

4.1. Crystallographic orientation

Mössbauer spectroscopy provides information on the crystallographic orientation of magnetically ordered single crystals. For a magnetic sextet from a single crystal:

$$A_{23} = 4(1-\cos^2\theta)/(1+\cos^2\theta), \quad (1)$$

Author's personal copy

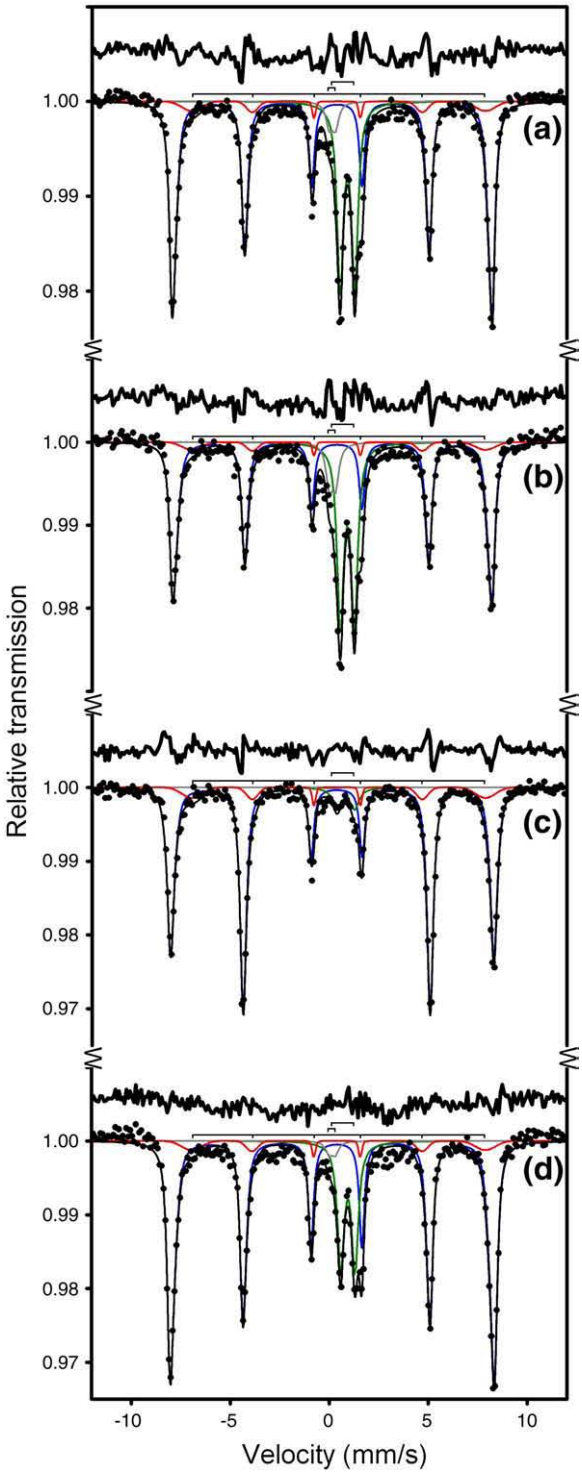

Fig. 3. Room-temperature Mössbauer spectra of natural ilmeno-hematite: (a) S17.2 (grain #2); (b) S19.5 (grain #2); (c) AD-34-1 (grain #2); (d) S47-3. All spectra show magnetically-ordered Fe^{3+} and $Fe^{2.5+}$ in titanohematite (blue and red online, respectively) and paramagnetic Fe^{2+} and Fe^{3+} in ilmenite (green and grey online, respectively). Line positions are shown as follows above each spectrum (top to bottom): Fe^{2+} in ilmenite doublet, Fe^{3+} in ilmenite doublet, $Fe^{2.5+}$ in hematite sextet. The intensity ratios of the magnetic spectra are close to the ideal 3:2:1:1:2:3 in all spectra except for spectrum (c), which shows a preferred orientation of the magnetic quantisation axis relative to the γ-ray direction. Some of the residuals (plotted above each spectrum on the same vertical scale) suggest the presence of an additional broad magnetic component, most notably spectrum (d). (For interpretation of the references to color in this figure legend, the reader is referred to the web version of this article.)

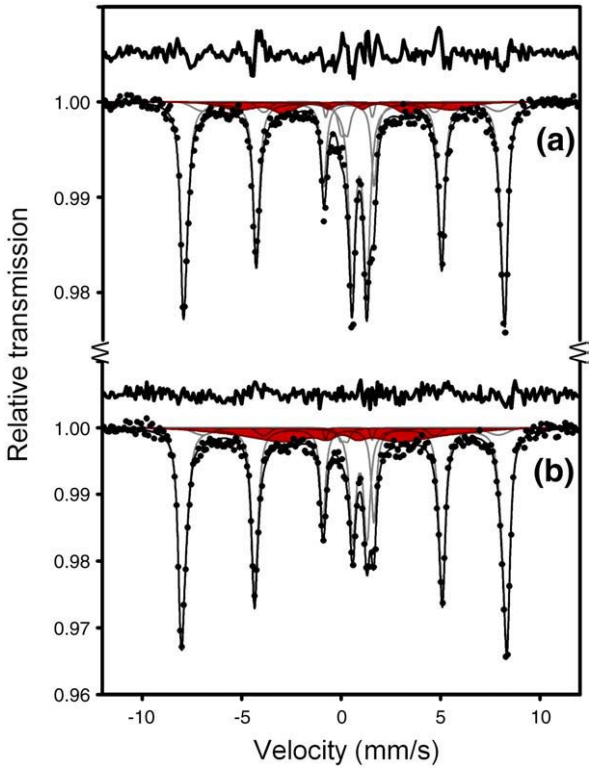

Fig. 4. Room-temperature Mössbauer spectra of natural ilmeno-hematite refitted including a broad magnetic component (shaded grey; red online): (a) S17.2 (grain #2); (b) S47-4. The presence of the component was found to be statistically significant to at least the 99% level in both spectra, although the hyperfine parameters cannot be uniquely determined. For the fits shown, the relative areas of the broad magnetic component in the upper and lower spectra are 9% and 16%, respectively. We suggest that the component corresponds to iron in contact layers. (For interpretation of the references to color in this figure legend, the reader is referred to the web version of this article.)

where θ is the angle between the γ-ray direction and the magnetic quantisation axis (e.g., Gütlich et al., 1978). For polycrystalline absorbers the magnetic vectors are averaged over all possible directions, giving the value $A_{23} = 2.0$ in the ideal case. The Mössbauer spectra of most grains from the present study gave A_{23} values close to 2, although several A_{23} values are above 3 (Table 1). The most probable explanation for the difference in A_{23} values relates to the fact that the grains analysed using Mössbauer spectroscopy likely approximate single crystals, similar to observations for hemo-ilmenite from South Rogaland, Norway (Robinson et al., 2006a). The grains selected were those which showed the sharpest exsolution features, and since rhombohedral oxide lamellae are constrained to exsolve within the basal plane (Robinson et al., 2002), thin sections tended to be oriented with the basal plane roughly perpendicular to the surface of the thin section (Fig. 5). The magnetisation vector lies in the basal plane due to the absence of the Morin transition, and should be quasi-parallel to one of the *a*-axes (Robinson et al., 2006a). Since the γ-ray is always oriented perpendicular to the plane of the thin section, the value of θ (Eq. (1)) depends on the angle between the γ-ray and one of the *a*-axes (Fig. 5). Therefore for a single crystal with a single magnetic domain with the (0001) plane exactly perpendicular to the plane of the thin section, we would observe a single A_{23} value. In reality, however, there may be different magnetic domains where the sublattice magnetisation in each domain may be parallel to a different *a* axis within the crystal, and there could also be crystallographic twins along a direction normal to the basal plane, which would give a sufficient number of different θ values to approximate the polycrystalline case of $A_{23} \approx 2$. For the two spectra where $A_{23} > 3$, this could arise from a more oblique orientation of the

Author's personal copy

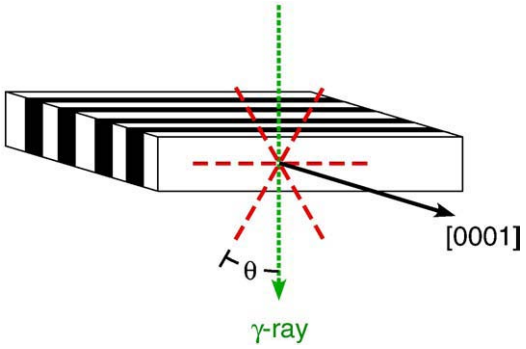

Fig. 5. Schematic diagram of an ilmeno-hematite thin section consisting of a titanohematite host (unshaded) containing ferri-ilmenite lamellae (black). Grains studied using Mössbauer spectroscopy were chosen as those showing the sharpest exsolution features, which occurs when the *c*-axis (black arrow) lies within the plane of the thin section. The A_{23} ratio is determined by the angle θ between the γ-ray (dotted arrow; green online) and the magnetisation vector (Eq. (1)), which for titanohematite above the Morin transition is quasi-parallel to one of the *a*-axes (dashed lines; red online) (Robinson et al., 2006b). (For interpretation of the references to color in this figure legend, the reader is referred to the web version of this article.)

(0001) planes in the thin section such that the γ-ray direction is closer to being parallel to the [0001] direction, or it could arise if a single *a*-axis contained the dominant sublattice magnetisation and it were nearly perpendicular to the γ-ray. The A_{23} ratio reaches its maximum value of 4.0 for γ-ray propagation exactly along [0001] ($\theta = 90°$).

4.2. Bulk composition

Mössbauer spectroscopy probes the atomic environment on a short-range scale. The hyperfine parameters measured by the Mössbauer effect are sensitive to at most the second next-nearest-neighbour shell, which means a scale of less than 0.4 nm for titanohematite, in contrast to TEM measurements which were made with a spatial resolution of 1–3 nm (McEnroe et al., 2001; Kasama et al., 2004) and electron microprobe data with a spatial resolution of several μm. We calculated the "ilmenite" ($R^{2+}Ti^{4+}O_3$) proportion of the titanohematite host and of the ferri-ilmenite lamellae from the area ratios of the individual Mössbauer components, and allowed for the small amount of Mg, Mn, V and Al determined by electron microprobe and analytical TEM. In nearly all grains the compositions of the titanohematite host and ilmenite lamellae determined by Mössbauer spectroscopy were significantly closer to end-member compositions compared to the range determined by electron microprobe and TEM on other grains within the same rock sample (Table 2), which is consistent with the observation that the range of lamellae widths extends as low as the nm length scale (e.g., McEnroe et al., 2001). We note that while compositions are closer to the end-members according to Mössbauer data, there is clear evidence that they do indeed deviate from end-member compositions based not only on the area ratios, but also on the reduced hyperfine magnetic field and broadened components of Fe^{3+} (Table 1). We therefore confirm the presence of Ti in titanohematite and Fe^{3+} in ferri-ilmenite even at the atomic scale.

Mössbauer spectroscopy also provides a means of determining the bulk composition of the assemblage, which is not easily obtained from any other method. The relative areas provide not only the $Fe^{3+}/\Sigma Fe$ ratios of the individual phases, but also the relative proportion of the phases themselves, which we used according to the lever rule to calculate the bulk "ilmenite" composition of each ilmeno-hematite grain. Results show that the bulk compositions of the Swedish samples are significantly more ilmenite-rich than the Adirondack samples (Table 2). For comparison, we calculated the modes of titanohematite and ferri-ilmenite (Fig. 1d) through point counting, with 3504 points. The bulk composition calculated from the point-counted modes combined with the electron microprobe analyses of individual phases is 40% "ilmenite", which is consistent with the value of $36 \pm 5\%$ calculated from the Mössbauer area ratios, particularly considering that electron microprobe data likely overestimates the "ilmenite" content of titanohematite. Bulk compositions determined by Mössbauer spectroscopy therefore provide a reliable method to estimate the bulk composition of individual grains. Uncertainties represent one-σ statistics of simultaneously minimising residuals for the Mössbauer data and the model.

4.3. Abundance of contact layers

The present study of ilmeno-hematite has shown that the Mössbauer data have many of the same properties as those reported earlier for igneous hemo-ilmenite (Dyar et al., 2004; Frandsen et al., 2007). In particular, Mössbauer spectra show no evidence of superparamagnetic (SPM) behaviour, which would appear as an additional quadrupole doublet in the spectrum. This observation confirms magnetic property measurements indicating that small nanoscale (<20 nm) hematite lamellae appear to be magnetically stable. The Mössbauer spectra also indicate that extremely small SPM or single domain magnetite grains are not present (these would also appear as additional quandrupole doublets, for which there is no evidence in the Mössbauer spectra); hence supporting the concept of lamellar magnetism in both types of samples; ilmenite hosts with hematite lamellae (hemo-ilmenite) and hematite hosts with ilmenite lamellae (ilmeno-hematite). We suggest that the broad magnetic component found in our spectra (shaded magnetic component in Fig. 4) is the same as the ferrimagnetic component originally identified by Frandsen et al. (2007) in their low-temperature spectra. Since our spectra were taken from single grains, we can rule out that the contribution comes from an impurity phase that Frandsen and colleagues could not absolutely exclude from powdered samples of hemo-ilmenite with rare silicate inclusions. The most likely explanation for the broad magnetic component is the suggestion of Frandsen et al. (2007) that it arises from iron in the contact layers, which are postulated to contain a mixture of Fe^{2+} and Fe^{3+} (Robinson et al., 2002, 2004; Harrison, 2006). The estimated thickness of the contact layers (≈0.23 nm; Robinson et al., 2006b) is challenging to be imaged even using TEM. However the size of the contact layers is easily within the range that can be detected by Mössbauer spectroscopy.

The identification of iron in the contact layers provides a means to estimate its proportion, and hence to obtain a rough estimate of the contact layer abundance. We followed the theoretical approach of Robinson et al. (2004) by constructing simulation cells of ilmenite lamellae in a titanohematite host consisting of either 24, 36, 48 or 72 layers with differing numbers of lamellae and compositions (Fig. 6). We assumed the ilmenite lamellae and titanohematite host to have the compositions Ilm100 and Ilm10, respectively, and calculated the average composition of the contact layers to be 0.525 Fe^{2+}, 0.45 Fe^{3+} and 0.025 Ti^{4+} based on a 50:50 ratio of Ilm100 to Ilm10. For each bulk composition we calculated the density of contact layers as a function of the proportion of iron in the contact layers (one example is given in Table 3), and the results are summarised in Fig. 7. For the spectrum with the highest proportion of iron in contact layers (S47-3 shows ≈16% $Fe_{CL}/\Sigma Fe$), the model gives a contact layer abundance of roughly 13.5% for the observed bulk composition (Ilm_{36}; Table 3). Prior to this work such an abundance has never been measured directly, only postulated.

4.4. Efficiency of lamellar magnetism calculated from NRM and lamellar models

An important practical ramification of the Mössbauer spectroscopy results is the possibility to estimate the efficiency of lamellar

Author's personal copy

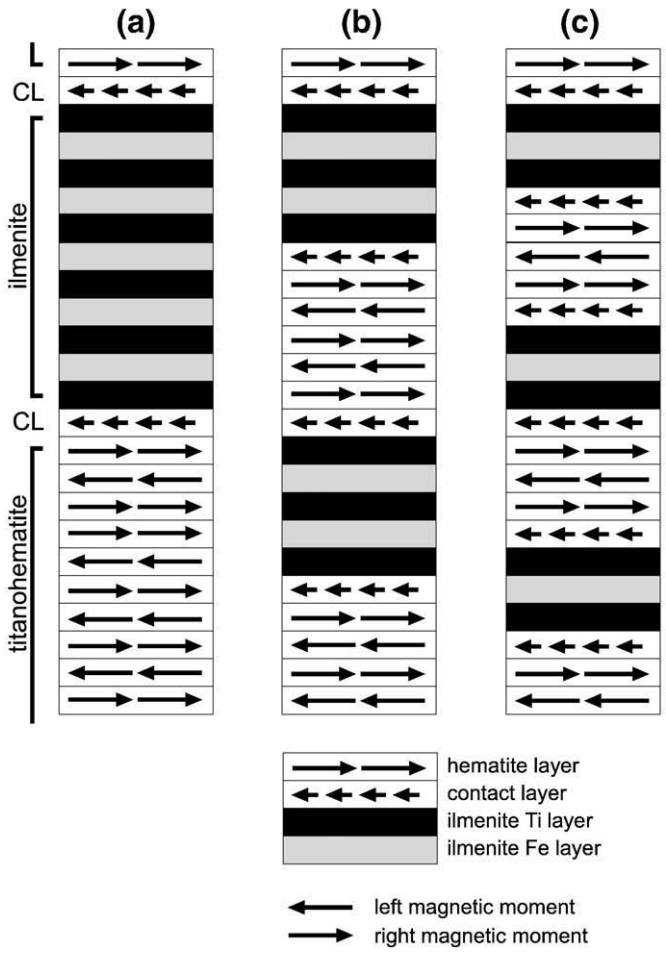

Fig. 6. Schematic illustration of 24-layer models of hematite containing (a) one ilmenite lamella two unit cells thick; (b) two ilmenite lamellae each one unit cell thick; (c) three ilmenite lamellae each 2/3 unit cell thick. All of these models have the same bulk composition, Ilm_{55}, but with differing numbers of lamellae. The bulk compositions of the models are Ilm_{55} for a hematite layer composition of Ilm_{10} and an ilmenite composition of Ilm_{100}. Each model is constructed so that the top layer is compositionally and magnetically compatible with the bottom layer, creating a "wrap-around effect" (after Robinson et al., 2004).

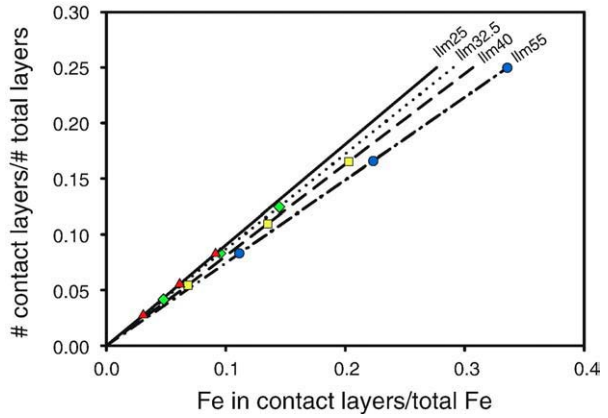

Fig. 7. Relative abundance of contact layers as a function of the amount of iron in the contact layers for four different bulk compositions: ilm_{25} (solid line with triangles; red online); ilm_{32} (dotted line with diamonds; green online); ilm_{40} (dashed line; with squares; yellow online); ilm_{55} (dashed-dotted line with circles; blue online). For ilm_{55}, values were determined using a 24-layer model as illustrated in Fig. 6 and listed in Table 3. A 36-layer model was required for ilm_{40}, and 48 layers and 72 layers were required for $ilm_{32.5}$ and ilm_{25}, respectively. The relative abundance of contact layer iron is higher in more ilmenite-rich samples due to the smaller amount of total iron. (For interpretation of the references to color in this figure legend, the reader is referred to the web version of this article.)

remanence acquisition. The efficiency R quantifies which fraction of the maximum possible (saturation) remanence is aligned by the NRM acquisition process. We calculated efficiencies in two equivalent ways, first from a microscopic perspective considering a model of atomic layers, and second by a mathematically simpler method using only bulk measurements and parameters, and show that both methods yield the same results.

For a single crystal and constant magnetic intensity the efficiency is related to the crystal orientation with respect to the magnetising field during exsolution. The maximum efficiency of 100% is likely when the (0001) basal plane is parallel to the magnetising field ($\alpha = 0°$) and will decrease according to cos α to a value of 0% when the magnetising field is perpendicular to the basal plane ($\alpha = 90°$). The samples studied here are not single crystals, but aggregates of crystals in solid rocks dominated by non-magnetic silicates. In natural samples, the NRM is a vector sum of all the magnetic moments and will depend on factors such as a strong lattice-preferred orientation (LPO) and its orientation with respect to the magnetising field. Without a LPO, the NRM (on a theoretical basis) will be 1/3 of the maximum magnetisation of a single crystal within the aggregate that is oriented with its (0001) plane parallel to the magnetising field. Intensities in A/m are therefore reduced to 1/3 if the rock has no LPO.

The lamellar magnetic moment is proportional to the number of magnetically in-phase lamellae and is essentially 4 μ_B per lamella (at 0 K) divided by the number of formula units (fu) of oxide in the model considered, where a formula unit consists of one atom in each of two layers (not the same as a unit cell which contains 12 atoms in 6 layers). The lamellar moment lies within the (0001) rhombohedral basal plane, the same plane containing the hematite sub-lattice magnetisations. The lamellar moment is independent of bulk composition, except to the extent that bulk composition plays a role

Table 3
Cation distribution in three 24-layer models of hematite (ilm_{10}) containing ilmenite (ilm_{100}) lamellae, all with bulk composition Ilm_{55}.

Layer	(a) One lamella				(b) Two lamellae				(c) Three lamellae			
	#layers	Ti	Fe^{3+}	Fe^{2+}	#layers	Ti	Fe^{3+}	Fe^{2+}	#layers	Ti	Fe^{3+}	Fe^{2+}
Ilmenite Ti	6	6	0	0	6	6	0	0	6	6	0	0
ilmenite Fe	5	0	0	5	4	0	0	4	3	0	0	3
hematite	11	0.55	9.9	0.55	10	0.5	9	0.5	9	0.45	8.1	0.45
contact layer (CL)	2	0.05	0.9	1.05	4	0.1	1.8	2.1	6	0.15	2.7	3.15
TOTAL	24	6.60	10.8	6.60	24	6.6	10.8	6.6	24	6.6	10.8	6.6
FeCL/ΣFe	0.112				0.224				0.342			
%CL	8.3				16.7				25.0			
bulk composition (x_{Ilm})	55				55				55			

Author's personal copy

in determining lamellar interface abundance during exsolution. If two lamellae are magnetically out-of-phase, then their moments cancel and contribute no lamellar magnetic moment. In considering the numbers for magnetic moment (per fu), it is convenient to consider a model with even numbers of lamellae and then to subtract them away in pairs to understand the progressive decrease in magnetic moment.

The first procedure we used to calculate efficiency of lamellar magnetism in these samples is presented in Table 4 (A–Q). Using the NRM values measured from the bulk sample (Table 4-A) and the point-counted volume fraction of rhombohedral oxide (Table 4-B), we calculate the NRM normalised to 100% rhombohedral oxide (Table 4-C). From the Mössbauer estimates of Fe_{CL}/Fe_{Total} (Table 4-D) and of bulk ilmenite composition (Table 4-E), we determine the ratio $Atomic_{CL}/Atomic_{Total\ Layers}$ from Fig. 7 (Table 4-F). This ratio is then multiplied (Table 4-G) in order to construct atomic models. The multipliers are used to produce models fulfilling the following requirements: 1) the number of lamellae must be an even integer, and 2) the model must have the same ratio $Atomic_{CL}/Atomic_{Total\ Layers}$ as in row F. Such models give a representation of a small segment of material in each sample with average properties within the real sample that must include thousands to millions of lamellae and layers. For sample S47 the model has 108 contact layers (Table 4-H) contained in 54 lamellae (Table 4-I) within a model 800 layers thick (Table 4-J) which contains 400 formula units (Table 4-K).

The rationale behind this approach is that the simplest model, with a line of atoms parallel to the *c*-axis, must have at least one atom in each layer, and a formula unit of rhombohedral oxide contains two atoms in two layers. A 'lamella' would consist of two average Fe^{2+}–Fe^{3+} contact layers each with a magnetic moment of 4.5 μB, intervening ilmenite with no magnetic moment, and the remaining hematite with one unbalanced magnetic moment of 5 μB in the opposite direction from the two contact layers. Thus, the magnetic moment of one lamella approximately equals $(2\times4.5\ \mu B)-(1\times5\ \mu B)=4\ \mu B$.

An alternative to the above is to consider a model in which each layer parallel to (0001) covers the area of a unit cell and always contains two atoms. For a Fe^{2+}–Fe^{3+} contact layer the magnetic moment is $4\ \mu B+5\ \mu B=9\ \mu B$. For a Fe^{3+}–Fe^{3+} hematite layer it is $2\times5\ \mu B=10\ \mu$. For a lamella, regardless of thickness, the moment in this model with 2 atoms per layer is $(2\times9\ \mu B)-(1\times10\ \mu B)=8\ \mu B$.

In the model for sample S47 with 800 layers containing 54 lamellae which are magnetically in-phase, i.e., 100% efficiency of magnetisation, the theoretical NRM at 0 K is $(54\times4\ \mu B)/400\ fu=0.54\ \mu B$ (Table 4-L). This NRM is converted into A/m by multiplying the numerical value of 0.54 μB by ≈183,000 A/m (Table 4-M). The conversion derives from the value of 1 μB ($9.274\times10^{-24}\ Am^2$) divided by the approximate volume per formula unit of rhombohedral oxide ($0.05\times10^{-27}\ m^3$), which takes into account the very dense atomic packing of this phase (Robinson et al., 2004). The same amount of material with the same proportion of contact layers could be placed within a single lamella in a thinner, but wider model, without any reduction in NRM. Models with a smaller fraction of atoms in contact layers will have smaller magnetic moments for the same "% efficiency".

The natural 100% oxide normalised NRMs (Table 4-C) are then divided by the calculated NRMs for 100% efficiency (Table 4-M) to give a ratio (Table 4-N). This ratio is multiplied by 100% to give the final % efficiency (Table 4-O), assuming that all of the crystals with their % efficiency are oriented in parallel, i.e., a perfect lattice-preferred orientation in the rock. When the same crystals are randomly oriented, the NRM is 1/3 of what it would have been with perfect orientation. Thus, the denominator of the ratio is divided by 3 (Table 4-P), yielding efficiency values that are three times larger (Table 4-Q).

4.5. Efficiency of lamellar remanence calculated from volume magnetisation and surface moment

A mathematically more direct approach to evaluating efficiency is provided by examining the volume magnetisation contained within the measured proportion of contact layers (Table 4: R–V). The contact layer abundance determined from Mössbauer data, combined with magnetic measurements, can be used to calculate the efficiency of magnetisation of the samples in acquiring a natural remanent magnetisation, assuming that the magnetisation is carried by lamellar magnetism. The bulk NRM is the magnetic moment per volume of a

Table 4
Two methods to calculate the efficiency of magnetisation.

		Sample			
	Unit	S47	S17	S19	AD34
Method 1					
A) Measured M_{NRM}	A/m	3.3	17.4	18.8	8.1
B) Rhombohedral oxide volume	%	0.5	3.1	3.0	1.8
C) NRM Normalised to 100% Oxide	A/m	660	561	627	450
D) Mössbauer estimate Fe_{Cl}/Fe_{Total}		0.16(5)	0.09(4)	0.10(6)	0.04(4)
E) Mössbauer Estimate of Bulk Composition		Ilm 36	Ilm 47	Ilm 48	Ilm 20
F)$Atomic_{Contact\ Layers}/Atomic_{Total\ Layers}$ from Fig. 7		0.134	0.071	0.075	0.035
(Simplified for Model)		(0.135)	(0.070)	(0.075)	(0.035)
G) Multiplier for Lamellar Model		800	400	800	800
H) Number of contact layers in model		108	28	60	28
I) Number of lamellae in model		54	14	30	14
J) Total Number of layers in model		800	400	800	800
K) Number of formula units in model		400	200	400	400
L) NRM pfu for 100% efficient model [(Number of Lamellae×4 μB)/fu]	μB	0.54	0.28	0.30	0.14
M) Conversion μB to A/m (×183,000 A/m) for 100% efficient model	A/m	98820	51240	54900	25620
N) NRM 100% Oxide/NRM Model (perfectly oriented crystals)		660/98820	561/51240	627/54960	450/25620
O) Efficiency = Ratio×NRM 100% (perfectly oriented crystals)	%	0.67	1.10	1.14	1.76
P) NRM 100% Oxide/NRM Model (randomly oriented crystals)		660/32940	561/17080	627/18320	450/8540
Q) Efficiency = Ratio×NRM 100% (randomly oriented crystals)	%	2.00	3.29	3.42	5.27
Method 2					
R) measured M_{NRM}	A/m	3.3	17.4	18.8	8.1
S) rhombohedral oxide volume (C_{Rh})	%	0.5	3.1	3.0	1.8
T) $Atomic_{Contact\ Layers}/Atomic_{Total\ Layers}$ from Fig. 7 simplified for model (A_{CL})	%	13.5	7.0	7.5	3.5
U) Volume magnetisation of the contact layers (M_{CL})	A/m	4890	8020	8360	12860
V) Efficiency (R)	%	0.67	1.10	1.14	1.76

Author's personal copy

sample, denoted by M_{NRM} (Table 4-R). The mode, C_{Rh}, is the volume fraction of magnetic rhombohedral oxides in the sample (Table 4-S). The atomic fraction (A_{CL}) of the oxides ($\approx$ volume fraction) residing in contact layers between hosts and lamellae has been estimated from the Mössbauer data (Table 4-T). By assuming that all NRM results from lamellar magnetism and ignoring the extremely weak moment contributed from spin-canted hematite, the volume magnetisation M_{CL} of the contact layers is calculated as:

$$M_{CL} = M_{NRM} / (C_{Rh}\, A_{CL}). \quad (2)$$

This quantity can be directly compared to the theoretically predicted volume magnetisation M_{lam} of lamellar surface moments residing in a contact layer of thickness h_{CL}. The unit cells of hematite and ilmenite are six layers thick, and have heights of 13.747 Å and 14.086 Å, respectively. A single contact layer would thus have a height $h_{CL} = 2.3$ Å. The theoretical lamellar surface moment m_{lam} is calculated by dividing the uncompensated lamellar moment μ_{lam} of one unit cell by the rhombohedral area U related to the unit cell on (0001):

$$m_{lam} = \mu_{lam} / U. \quad (3)$$

According to Robinson et al. (2004), $\mu_{lam} = 4\,\mu_B$, which is derived from the fact that there are two Fe atoms within the unit cell area of an (0001) plane and there are two contact layers. This gives a net moment per lamella of this size of 8 μB, but when divided by two contact layers the final value is 4 μB. The area related to the unit cell on (0001) of the contact layer is a rhombus with sides of 5.048 Å with an angle of 60° between them, which yields

$$U = (5.048\text{Å})^2 \sin 60^\circ. \quad (4)$$

The theoretical volume magnetisation M_{lam} of the contact layers thereby becomes

$$M_{lam} = m_{lam} / h_{CL} = \mu_{lam} / U / h_{CL} = 731\,\text{kA/m}, \quad (5)$$

and from this we can infer the efficiency,

$$R = M_{CL} / M_{lam}. \quad (6)$$

of lamellar remanence acquisition for the four samples. The R values derived by this method (Table 4-V) lie between 0.6% and 1.8% and correspond exactly with the calculations by the previous method (Table 4-O).

4.6. Interpretation of the efficiency of lamellar remanence

The two calculation routes above yield mutually consistent values of efficiency between 0.7% and 1.8%. While the initial volume magnetisation of the samples varied by a factor of 6, the normalised efficiency varies only by a factor 3, indicating that remanence acquisition of the contact layers is equally efficient in different settings. Higher efficiency is observed if (a) the modal amount of oxide is less, if (b) the estimated fraction of magnetically stable contact layers is lowered, giving lower theoretical magnetisations for the same efficiency, or if (c) an LPO is weak or absent, reducing the theoretical efficiency compared to single crystals. The observed lamellar-remanence efficiency of $R = 1$–2% is large, even when compared to typical thermoremanent magnetisation (TRM) efficiencies $M_{TRM}(H_0)/M_S$ for ideal isotropic single-domain (SD) magnetite particles acquiring a thermoremanent magnetisation by cooling in the geomagnetic field H_0. The maximal TRM efficiency R_{TRM} for SD magnetite is estimated by using the theoretical TRM efficiency (Eq. (7.6) from Stacey and Banerjee (1974)) and estimating the temperature dependence of saturation magnetisation for magnetite as:

$$M_S(T) = M_{S,0}(1 - T/T_C)^{0.4}. \quad (7)$$

Here, T_C is the Curie-temperature of magnetite and $M_{S,0}$ is the saturation magnetisation at room temperature. R_{TRM} can then be estimated as:

$$R_{TRM} = M_{TRM}(H_0) / M_{S,0} = VH_0M_S(1 - T_B/T_C)^{0.4} / (3k_BT_B) < 3\%, \quad (8)$$

where the SD particle volume is approximately $V = (50\text{ nm})^3$, $M_{S,0} = 480$ kA/m, the thermal blocking temperature is taken as $T_B = 800$ K, and $T_C = 850$ K. More realistic efficiency values for grain-size distributions of SD particles yield values well below $R = 0.1\%$.

By comparing the Mössbauer spectroscopy results to the above value for SD magnetite TRM, it appears that lamellar magnetism may be the most efficient mechanism of natural remanence acquisition known to date. A previous estimate of lamellar NRM-alignment efficiency is based on low-temperature exchange bias (Fabian et al., 2008), and resulted in an efficiency ratio of $R_{EB} = 76\%$ (88% of the exchange bias moments aligned, 12% inverse). However, as discussed by Fabian et al. (2008), this high efficiency probably does not refer to alignment of individual lamellae, but to the alignment of the net moments of coupled clusters of lamellae, where each cluster contains lamellae with opposite orientations. Based on the value of $R \approx 2\%$, the probability of a single lamella to be aligned with the magnetising field is $p^* = (1 + R)/2 = 51\%$. If clusters with a number of such lamellae (N) lead to an exchange-bias efficiency $R_{EB} = 76\%$, the calculation in Fabian et al. (2008) gives $N \approx (p^* - ½)^{-2} \approx 10000$, a value already considered in this previous article.

The Mössbauer spectroscopy data indicate that the magnetic moments of nanoscale hematite lamellae contained within ilmenite lamellae are thermally stable, in contrast to hematite nanoparticles of the same size, which would be superparamagnetic. If the magnetism of these nanoscale lamellae were not thermally stable, then the number of stable contact layers would be lower, and the efficiency of the remaining magnetisation would have to be significantly higher to account for the NRM values.

4.7. Implications for remanent magnetic anomalies

Using the above finding that remanence acquisition of the contact layers has approximately a constant efficiency, it follows that the volume magnetisation of a rock produced by lamellar magnetism is proportional to the modal amount of exsolved rhombohedral oxide in the rock and to the contact-layer density, which in turn is proportional to the total surface area of the lamellae. The technique proposed here, which relates the contribution from the magnetic contact layers to a broad component of the Mössbauer spectrum not fitted to the spectra of synthetic titanohematite, is the only currently available method to measure contact layer density.

Because rocks with similar modal amounts of rhombohedral oxide but greater contact-layer density have higher NRM values than those with low contact-layer density, even rocks with only a few percent of rhombohedral oxides can have very high NRM values. Thus, the remanent magnetic anomalies over very similar rock types can vary considerably in intensity, depending on small variations in exsolution conditions.

Acknowledgments

A portion of the project was performed at the Bayerisches Geoinstitut under the EU "Research Infrastructures: Transnational Access" Programme (Contract No. 505320 (RITA) — High Pressure).

Author's personal copy

Research was also supported by the Research Council of Norway (RCN grants 189721/S10 and 169470/S30).

References

Balsley, J.R., Buddington, A.F., 1954. Correlation of reversed remanent magnetism and negative anomalies with certain minerals. J. Geomagn. Geoelectr. 6, 176–181.

Balsley, J.R., Buddington, A.F., 1957. Remanent magnetism of the Russell belt of gneisses, Northwest Adirondack mountains, New York. Adv. Phys. 6, 317–322.

Balsley, J.R., Buddington, A.F., 1958. Iron-titanium oxide minerals, rocks, and aeromagnetic anomalies of the Adirondack area, New York. Econ. Geol. 53, 777–895.

Bevington, P.R., 1969. Data reduction and error analysis for the physical sciences. McGraw-Hill, New York.

Burton, B.P., 1982. Thermodynamic analysis of the systems $CaCO_3$–$MgCO_3$, α-Fe_2O_3 and Fe_2O_3–$FeTiO_3$, Ph.D. thesis, State University of New York at Stony Brook.

Dyar, M.D., McEnroe, S.A., Murad, E., Brown, L.L., Schiellerup, H., 2004. The relationship between exsolution and magnetic properties in hemo-ilmenite: insights from Mössbauer spectroscopy with implications for planetary magnetic anomalies. Geophys. Res. Lett. 31. doi:10.1029/2003GL019076, 2004.

Ericsson, T., Krisnhamurthy, A., Srivastava, B.K., 1986. Morin transition in Ti-substituted hematite — a Mössbauer study. Phys. Scr. 33, 88–90.

Fabian, K., McEnroe, S., Robinson, P., Shcherbakov, V., 2008. Exchange bias identifies lamellar magnetism as the origin of the natural remanent magnetization in titanohematite with ilmenite exsolution from Modum, Norway. Earth Planet. Sci. Lett. 268, 339–353.

Frandsen, C., Mørup, S., McEnroe, S., Robinson, P., Langenhorst, F., 2007. Magnetic phases in hemo-ilmenite: insight from low-velocity and high-field Mossbauer spectroscopy. Geophys. Res. Lett. 34, L07306.

Gütlich, P., Link, R., Trautwein, A., 1978. Mössbauer spectroscopy and transition metal chemistry. Springer-Verlag, Berlin.

Harrison, R.J., 2006. Microstructure and magnetism in the ilmenite–hematite solid solution: a Monte Carlo simulation study. Am. Mineral. 91, 1006–1023.

Harrison, R., Becker, U., 2001. Magnetic ordering in solid solutions. EMU Notes Mineral. 3, 349–383.

Harrison, R., McEnroe, S., Robinson, P., Carter-Stiglitz, B., Palin, E., Kasama, T., 2007. Low-temperature exchange coupling between Fe_2O_3 and $FeTiO_3$: insight into the mechanism of giant exchange bias in a natural nanoscale intergrowth. Phys. Rev. B 76, 174436.

Ishikawa, Y., 1958. Electrical properties of the $FeTiO_3$–Fe_2O_3 solid solution series. J. Phys. Soc. Jpn. 13, 37–42.

Kasama, T., McEnroe, S.E., Ozaki, N., Kogure, T., Putnis, A., 2004. Effects of nanoscale exsolution in hematite–ilmenite on the acquisition of stable remanent magnetization. Earth Planet. Sci. Lett. 224, 461–475.

McCammon, C.A., Chaskar, V., Richards, G.G., 1991. A technique for spatially resolved Mössbauer spectroscopy applied to quenched metallurgical slags. Meas. Sci. Technol. 2, 657–662.

McEnroe, S.E., Brown, L.L., 2000. A closer look at remnanence-dominated aeromagnetic anomalies: Rock magnetic properties and magnetic mineralogy of the Russell Belt microcline–sillimanite gneiss, northwest Adirondack Mountains, New York. J. Geophys. Res. 105, 16437–16456.

McEnroe, S.E., Harrison, R.J., Robinson, P., Golla, U., Jercinovic, M.J., 2001. Effect of fine-scale microstructures in titanohematite on the acquisition and stability of natural remanent magnetization in granulite facies metamorphic rocks, southwest Sweden: Implications for crustal magnetism. J. Geophys. Res. 106, 30523–30546.

McEnroe, S., Harrison, R., Robinson, P., Langenhorst, F., 2002. Nanoscale haematite–ilmenite lamellae in massive ilmenite rock: an example of 'lamellar magnetism' with implications for planetary magnetic anomalies. Geophys. J. Int. 151, 890–912.

McEnroe, S., Carter-Stiglitz, B., Harrison, R., Robinson, P., Fabian, K., McCammon, C., 2007a. Magnetic exchange bias of more than 1 Tesla in a natural mineral intergrowth. Nature Nanotech. 2, 631–634.

McEnroe, S., Robinson, P., Langenhorst, F., Frandsen, C., Terry, M., Boffa-Ballaran, T., 2007b. Magnetization of exsolution intergrowths of hematite and ilmenite: mineral chemistry, phase relations, and magnetic properties of hemo-ilmenite ores with micron- to nanometer-scale lamellae from Allard Lake Quebec. J. Geophys. Res. 112, B10103.

Pentcheva, R., Nabi, H., 2008. Interface magnetism in Fe_2O_3/$FeTiO_3$ heterostructures. Phys. Rev. B 77, 172405.

Rancourt, D.G., Ping, J.Y., 1991. Voigt-based methods for arbitrary-shape static hyperfine parameter distributions in Mössbauer spectroscopy. Nucl. Instrum. Methods Phys. Res., Sect. B 58, 85–97.

Robinson, P., Harrison, R.J., McEnroe, S.E., Hargraves, R.B., 2002. Lamellar magnetism in the haematite–ilmenite series as an explanation for strong remanent magnetization. Nature 418, 517–520.

Robinson, P., Harrison, R.J., McEnroe, S.A., Hargraves, R.B., 2004. Nature and origin of lamellar magnetism in the hematite–ilmenite series. Am. Mineral. 89, 725–747.

Robinson, P., Heidelbach, F., Hirt, A., McEnroe, S., Brown, L., 2006a. Crystallographic–magnetic correlations in single-crystal haemo-ilmenite: new evidence for lamellar magnetism. Geophys. J. Int. 165, 17–31.

Robinson, P., Harrison, R.J., McEnroe, S.A., 2006b. Fe^{2+}/Fe^{3+} charge ordering in contact layers of lamellar magnetism: bond valence arguments. Am. Mineral. 91, 67–72.

Stacey, F.D., Banerjee, S.K., 1974. The Physical Princples of Rock Magnetism. Elsevier Scientific Publishing Company.

van der Woude, F., Dekker, A.J., 1966. Mössbauer effect in α-FeOOH. Phys. Status Solidi 13, 181–193.

Warner, B.N., Shive, P.N., Allen, J.L., Terry, C., 1972. A study of the hematite–ilmenite series by the Mössbauer effect. J. Geomagn. Geoelectr. 24, 353–367.